Insights into the Mechanical Characterization of Mouse Brain Tissue Using Microindentation Testing

Xuesong Zhang,[1] Eva A. N. van den Hurk,[1,2] and Johannes Weickenmeier[1,3,4]

[1]Department of Mechanical Engineering, Stevens Institute of Technology, Hoboken, New Jersey
[2]Department of Biomedical Engineering, Eindhoven University of Technology, Eindhoven, Netherlands
[3]Center for Neuromechanics, Stevens Institute of Technology, Hoboken, New Jersey
[4]Corresponding author: *johannes.weickenmeier@stevens.edu*

Indentation testing is the most common approach to quantify mechanical brain tissue properties. Despite a myriad of studies conducted already, reported stiffness values vary extensively and continue to be subject of study. Moreover, the growing interest in the relationship between the brain's spatially heterogeneous microstructure and local tissue stiffness warrants the development of standardized measurement protocols to enable comparability between studies and assess repeatability of reported data. Here, we present three individual protocols that outline (1) sample preparation of a 1000-µm thick coronal slice, (2) a comprehensive list of experimental parameters associated with the FemtoTools FT-MTA03 Micromechanical Testing System for spherical indentation, and (3) two different approaches to derive the elastic modulus from raw force-displacement data. Lastly, we demonstrate that our protocols deliver a robust experimental framework that enables us to determine the spatially heterogeneous microstructural properties of (mouse) brain tissue. © 2024 Wiley Periodicals LLC.

Basic Protocol 1: Mouse brain sample preparation
Basic Protocol 2: Indentation testing of mouse brain tissue using the FemtoTools FT-MTA03 Micromechanical Testing and Assembly System
Basic Protocol 3: Tissue stiffness identification from force-displacement data

Keywords: brain sample preparation • indentation testing • mechanical characterization • mouse brain tissue

How to cite this article:
Zhang, X., van den Hurk, E. A. N., & Weickenmeier, J. (2024). Insights into the mechanical characterization of mouse brain tissue using microindentation testing. *Current Protocols*, *4,* e1011. doi: 10.1002/cpz1.1011

INTRODUCTION

The mechanical properties of soft tissues are intricately linked to their physical and biological function (Budday et al., 2017; Hiscox et al., 2020; Murphy et al., 2012). Tissue stiffness, i.e., elastic modulus, in the human body typically ranges from about 1 kPa for a single cell (Luo et al., 2016) to about 1-10 kPa for many tissues and organs, such as the brain, cardiac tissues, and lung (Guimarães et al., 2020). Even though values vary throughout literature, average brain stiffness is between 1 and 3 kPa (Budday et al., 2020). The mechanical environment of individual cerebral tissues is intricately linked to local microstructure. Therefore, brain properties evolve throughout life ranging from

CURRENT PROTOCOLS
A Wiley Brand

Current Protocols e1011, Volume 4
Published in Wiley Online Library (wileyonlinelibrary.com).
doi: 10.1002/cpz1.1011

early neurodevelopment (when the folded cortex is formed), aging (gradual white and gray matter degeneration), and dementia (when toxic proteins accelerate neurodegeneration) (Blinkouskaya et al., 2021; Franze et al., 2013; Goriely et al., 2015; Hall et al., 2021; Meaney et al., 2014). It has been established that the brain is among the softest tissues in the human body and is characterized by a highly nonlinear, poroviscoelastic, and spatially heterogeneous mechanical response (Budday et al., 2020). Therefore, brain tissue testing is subject to many challenges that include access to samples, size of samples, complexity of the microstructure, reproducing physiological loading conditions, testing environment, and effectively establishing a better understanding of the relationship between microstructure and mechanical response (Faber et al., 2022). Additionally, despite extensive research efforts, the mechanical properties of brain tissue remain subject for debate with a wide range of values reported in literature (Budday et al., 2020).

Indentation testing is the most common approach to quantify mechanical brain tissue properties (Antonovaite et al., 2018; Budday et al., 2015; Christ et al., 2010; Gefen & Margulies, 2004; MacManus & Ghajari, 2022; Van Dommelen et al., 2010; Weickenmeier et al., 2016); yet, many experimental design factors vary between studies despite their significant impact on a realistic evaluation of the tissue's mechanical behavior. In addition, determination of tissue stiffness requires the evaluation of a model that is representative of the indentation loading case. Solutions exist for both linear and nonlinear material behavior and may be selected based on the user's particular case.

In the present work, we present three different protocols that provide a step-by-step guide ranging from sample preparation to stiffness determination for mouse brain tissue. Specifically, we outline how to prepare a 1000-μm thick brain slice, use the FemtoTools FT-MTA03 Micromechanical Testing System to perform spherical indentation (single measurements or grid measurements), and present two different strategies to derive tissue stiffness from the raw force-displacement data of a single measurement. We identify and discuss crucial experimental parameters that may have significant implications on measurement outcome and, lastly, present the results of a case study demonstrating the capabilities of our protocols to determine the spatially heterogeneous distribution of tissue stiffness across individual brain regions.

NOTE: All protocols involving animals must be reviewed and approved by the appropriate Animal Care and Use Committee and must follow regulations for the care and use of laboratory animals. Appropriate informed consent is necessary for obtaining and use of human study material.

BASIC PROTOCOL 1

MOUSE BRAIN SAMPLE PREPARATION

This protocol outlines how to prepare a coronal mouse brain slice at 0.7 mm anterior Bregma that provides access to various brain regions, including the corpus callosum, cingulum, and cortex. The protocol delivers a smooth 1000−μm thick tissue slice that is suitable for microindentation testing. In preparation for creating these slices, we fabricated a custom-built mouse brain mold made of PLA filament with overall dimensions 50 mm × 30 mm × 20 mm and a cut-out size of 19 mm × 11 mm × 7.5 mm, as shown in Figure 1. We printed the mold at a resolution of 100 μm and a layer thickness of 200 μm. In this protocol, we outline how to excise the brain, mount it in a vibratome to cut a 1000-μm thick slice, and transfer it to a petri dish for subsequent testing. This protocol may be easily modified to deliver samples from ultrasoft materials.

Materials

Mouse (we typically use 8-week-old C57BL/6 mice)
Phosphate-buffered saline (VWR, cat. no. 97064-158)
Super glue (Gorilla, cat. no. 7500101)

Surgical knife (Med-Vet International, cat. no. 50-118-0432)
Surgical scissors (Med-Vet International, cat. no. 50-209-2742)
Tweezer (DR Instruments, cat. no. S72112)
Paint brush (Aroic, model. no. Paintbrush Set A-10p)
Stainless steel flat-end spatula (United Scientific Supplies, cat. no. 76263-350)
Custom-built mold (see Figs. 3B and 2C) made using:
3D Printer (Prusa, MK3S)
Appropriate filament (e.g., Ultimaker Tough PLA filament)
Electrical tape (3M, cat. no. 19-072-072)
VT-1200S vibratome (Leica Microsystems, cat. no. NC1509842)
Stainless double-edge blade (AccuTec Blades, cat. no. 17-989-043)
Kimwipes (Kimtech Science, cat. no. 06-666)
Disposable petri dish (Benz Microscope, cat. no. P32223)
Transfer pipet (Global Scientific, cat. no. 89209-802)

Excise mouse brain

1. Use cervical dislocation to sacrifice the mouse.
2. Cut the head from the mouse carcass and use scissors to cut and remove the skin (Fig. 2A).

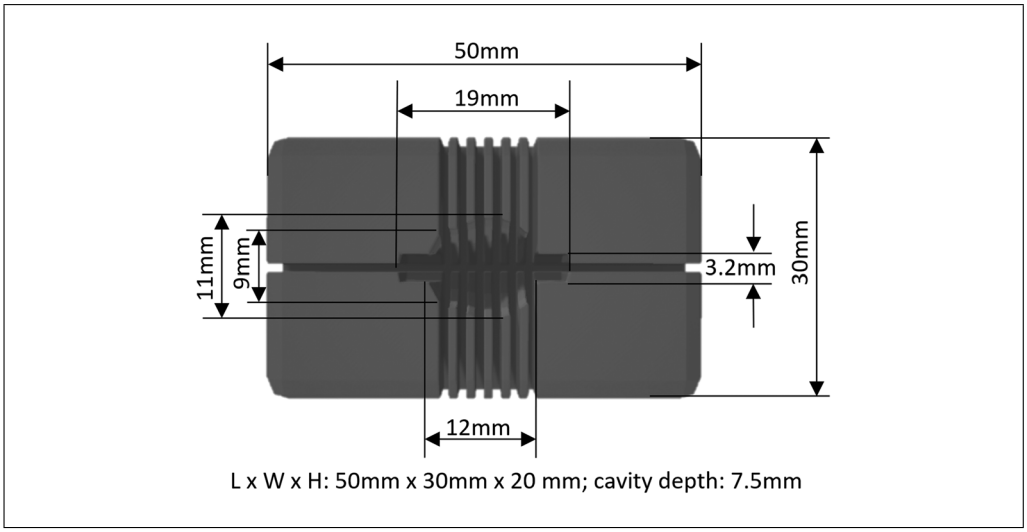

Figure 1 The structure and dimensions of the custom-built cutting mold used for preparing the mouse brain slice.

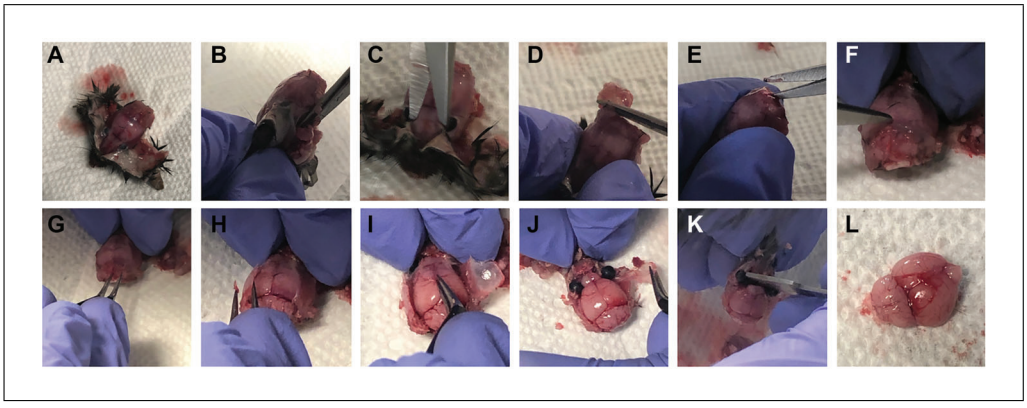

Figure 2 Brain harvesting procedures: (**A**) remove the skin of the mouse head, (**B**) cut off the temporal muscles, (**C**) cut off the bones in between the eyes, (**D**) remove the spinal cord, (**E**) create a crack along with sagittal suture that exceeds lambda point (**F**), flip the parietal bones (**G-H**) and frontal bones (**I-J**), and remove the brain from the skull (**K-L**).

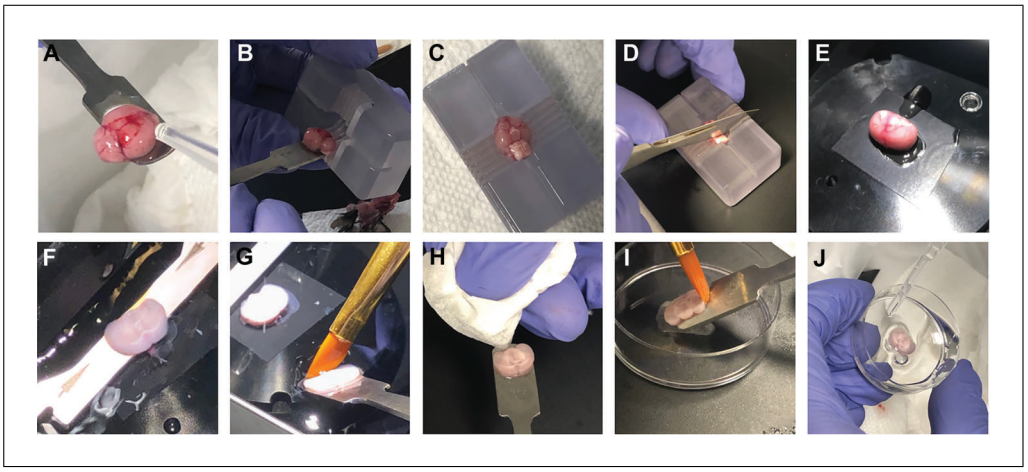

Figure 3 Slice cutting procedures: (**A**) rinse the brain using PBS, (**B-C**) and transfer the brain to the cutting mold, (**D**) remove the cerebellum, (**E**) glue the brain sample to vibratome disc, (**F**) cut a 1-mm slice at 0.7 mm anterior Bregma, (**G**) take the sample out of the vibratome, (**H**) absorb the liquid around the sample, (**I**) glue the sample to a petri dish, and (**J**) use extensive PBS to rinse the sample.

3. Cut away the temporalis muscle on both sides of the skull (Fig. 2B).
4. Cut the bone between the eyes (Fig. 2C).
5. Cut away the remaining spinal cord (Fig. 2D).
6. Cut the skull with scissors to create a crack in the occipital bone that runs along the sagittal suture (Fig. 2E) until the crack reaches the lambda point (Fig. 2F).
7. Use tweezers to break away the parietal bone (Fig. 2G and 2H) and frontal bone (Fig. 2I and 2J).
8. Use a brush and spatula to gently extract the brain from the skull (Fig. 2K and 2L).
9. Use the spatula to transfer the brain that is rinsed with phosphate-buffered saline (PBS) solution (Fig. 3A) to the custom-built mold (Fig. 3B and 2C).

   NOTE: *The ventral surface of the mouse brain should face upwards, and the dorsal surface should face downwards.*

10. Use a surgical knife to remove the cerebellum by cutting at the second gap from the right of the mold (Fig. 3D).

Transfer the brain to the vibratome

11. Stick a quarter-sized patch of electrical tape onto the vibratome disc.
12. Remove the brain from the mold and glue the brain onto the electrical tape using superglue (Fig. 3E).
13. Assemble the stainless double edge blade of the vibratome, transfer the disc to the container of the vibratome machine, and fill the container with PBS stored at 4°C.
14. Prepare a 1000-µm thick brain slice with two cuts at 0.7-mm anterior Bregma and 1.7-mm anterior Bregma (Fig. 3F).
15. Use the brush and spatula to remove the brain slice from the vibratome container (Fig. 3G).
16. Use a Kimwipe to absorb the liquid around the sample (Fig. 3H).

    NOTE: *This step removes excess PBS to ensure better adhesion of the sample to the petri dish in the next step.*

Glue the brain slice into the petri dish

17. Apply a thin, even layer of superglue at the center of the petri dish and glue the slice to the petri dish (Fig. 3I). Wait 1 minute for the glue to dry.

18. Use a pipette to rinse the sample with PBS and remove all residuals from previous steps (Fig. 3J).

INDENTATION TESTING OF MOUSE BRAIN TISSUE USING THE FEMTOTOOLS FT-MTA03 MICROMECHANICAL TESTING AND ASSEMBLY SYSTEM

BASIC PROTOCOL 2

Indentation testing is a well-established method for the mechanical characterization of biological materials (Budday et al., 2015; Moghaddam et al., 2023; Weickenmeier et al., 2016; Zhang & Weickenmeier, 2023) and various indentation devices are commercially available. The following protocol is specific to the FemtoTools FT-MTA03 Micromechanical Testing and Assembly System (FemtoTools, Buchs CH) but may be easily modified to other systems as many of the experimental parameters are common inputs for indentation measurements. This protocol outlines the protocol for quasi-static indentation of mouse brain tissue. Specifically, we describe how to glue a microsphere to the flat rectangular tip of the FemtoTools FT-S Microforce Sensing Probe (FemtoTools, Buchs, Switzerland) to enable spherical indentation, specify machine and user interface software settings, and outline all relevant indentation parameters. The protocol presented here may easily be extended to testing other biological materials as well.

Materials

Petri dish with brain sample (see Basic Protocol 1)
50-μm diameter Polystyrene microsphere bead (Alpha Nanotech; size subject to application)
Contact lens solution (Opti-free, Alcon Laboratories, item model no. 65035721)

FT-MTA03 Micromechanical Testing System (FemtoTools AG, Buchs, Switzerland)
FT-S200 Microforce Sensing Probe (FemtoTools AG, Buchs, Switzerland)
Transfer pipet (Global Scientific, cat. no. 89209-802)
Microscope glass slide (Global Scientific, cat. no. 1304)
Light cure adhesive (Loctite, AA-3491)
Ultraviolet flashlight (Lightfe, UV301d)

Gluing a bead to the tip of force sensor

1. Start FT-MTA03 Micromechanical Testing System Control Software.

2. In the Simple Indentation Module, select the positive Z direction as the indentation direction and initialize the piezoscanner and nanopositioner.

3. In the pop-up window, select the tip type as spherical with a bead radius of 25 μm and the reference stiffness as infinity. Then, the main interface automatically shows up (Fig. 4A).

4. Open three monitoring windows from the software interface to track the real-time position and force recordings from the sensor during idle-time and the indentation process.

   NOTE: *We recommend monitoring the Tip Position in Z direction, Piezo Position in Z direction, and Sensor Tip Force (Force A) to ensure that sensor recordings are nominal (Fig. 4B).*

5. Rotate the internal microscope to 80° on one side and place the support lighting on the opposing side of the stage.

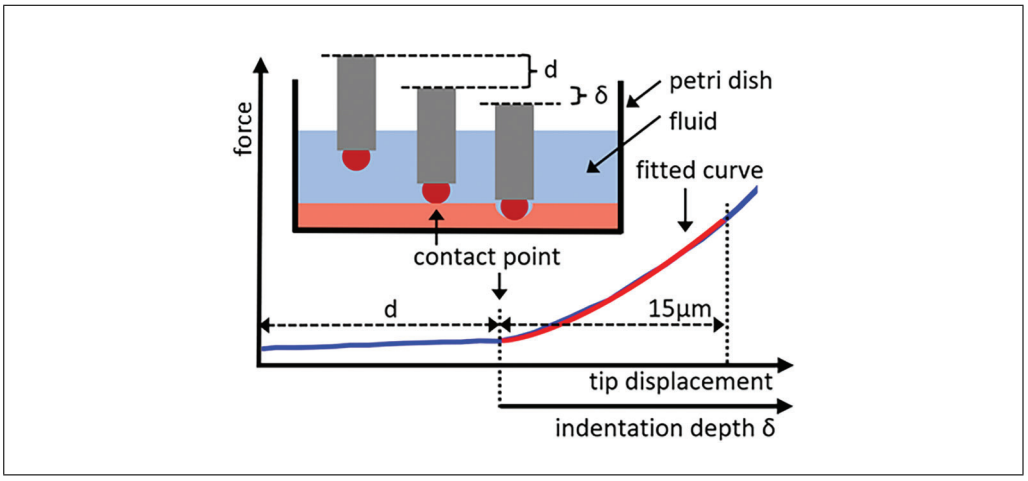

Figure 4 Schematic of the testing process, (**A**) the main interface of the software, (**B**) the monitoring window of piezo-position *Z*, stage-position *Z*, and indenter force A, where the green line indicates the mean value of each window in a timeframe of 5 s, (**C**) the setup of the sample in the machine, (**D**) the sensor and sample engagement, and (**E**) a schematic of the 6 × 6 measurement grid with an inter-measurement spacing of 75 µm; the red line indicates the direction in grid testing.

6. Use a transfer pipette to place several polystyrene microsphere beads on a microscope glass slide.
7. Use a new transfer pipette to place a small amount of light cure adhesive next to the beads on the glass slide.
8. Place the glass slide on the stage of the machine.
9. Use the internal microscope to locate a well-isolated bead and move the sensor until the tip is above the targeted bead.

   NOTE: *The vertical center line of the tip should coincide with the vertical center line of the bead. Carefully move the sensor tip as close to the bead as possible without contact to ensure best alignment prior to gluing.*

10. Use the "Find Contact" function to determine the contact point between tip and bead. Function settings: 5 µm/s speed, 3 µN maximum force, 3000 Hz filter, and 20 µm move-back distance.

    NOTE: *The highest point of the bead should contact the lowest flat surface in the microscope; otherwise, use 1-µm step size to move the sensor in Y direction (forward or backward).*

11. Save the current sensor position and raise the sensor by 2000 µm.
12. Move the sensor until the tip is above the light cure adhesive.
13. Manually move the sensor tip towards the surface of the adhesive; when the tip dips 1-µm into the adhesive, wait for 3 s, then raise the sensor by 2000 µm.
14. Return the sensor to the saved position (step 10), set the move-back distance to 0 µm, and use the "Find Contact" function for tip and bead to touch.
15. Wait 5 s, and then raise the tip by 50 µm.
16. Use the ultraviolet flashlight to cure the adhesive glue between tip and bead for 1 min.
17. Remove the glass slide from the stage.

Indentation testing on a grid with step annotations

18. Place the petri dish with brain sample on the testing stage (see Basic Protocol 1).

19. Pipette contact lens solution (at room temperature or approximately 21°C) to the petri dish until the entire slice is marginally submerged.

    NOTE: *We use contact lens solution because it reduces adverse interaction forces between the indenter tip, submersion fluid, and tissue. Other surfactants may be explored for other applications.*

    NOTE: *We recommend conducting experiments at room temperature (approximately 21°C). If all measurements are completed within 1-2 hr of sacrificing the animal, measurement results are not affected by temperature (if at or below room temperature) and do not require to be actively cooled.*

20. Use the following set of "Find Contact" parameters:

    Direction: Pos Z-
    Distance: 1E+6 [μm]
    Speed: 100 [μm/s]
    Move Back: 40 [μm]
    Min Force: -15 [μN]
    Max Force: 3 [μN]
    Filter: 2000 [Hz]
    Sidestep Pos X: 50 [μm]
    Sidestep Pos Y: 0 [μm]

21. Use the following set of "Test Indentation" parameters:

    Direction: Pos Z+ (up)
    Control Mode: position controlled
    Distance: 25000 [μm]
    Trigger Min: -10 [μN]
    Filter: 6 [Hz]
    Trigger Max: 0.3 [μN]
    Approach Step: 40 [μm]
    Approach Speed: 10 [μm/s]
    Approach Wait: 0.1 [s]
    Following Step: 30 [μm]
    Following Speed: 200 [μm/s]
    Max Force: 20 [μN]
    Max Depth: 15 [μm]
    End Force: -500 [μN]
    Sampling Rate: 40 [Hz]
    Load Ramp Time: 1.5 s
    Unload Rate Time: 0.02 s
    Loaded Hold Time: 0 s
    End Hold Time: 0 s

    NOTE: *The load ramp time and unload ramp time control the tip speed during the loading and unloading phase, respectively. In our applications, we use a very short unload ramp time because we are not interested in the unloading data. This can easily be adjusted for other applications.*

22. Use the following set of "Array" parameters:

    Conduct measurements as: an array in direction A&B from the sensor
    Max Indent Depth: 15 [μm] to 15 [μm]
    Skip Find Contact: yes

Logarithmic: no
Depth Variation Direction: Pos X+ (right)
Repetition Direction: Pos Y+ (back)
Number of Subdivisions: 6
Number of Repetitions: 6
Indent Spacing: 75 [μm]
Const. Ramp Time
Zero Force Before Each Indentation: yes
Move Back: Pos Z+ (up)
Distance: 0 [μm]
Speed: 500 [μm/s]
Delay Before Measurement: 0.5 s

NOTE: *The number of subdivisions, repetitions, and indent spacing can be adjusted based on your desired measurement grid.*

NOTE: *The "Zero Force" function is very useful to reset the tip force reading, which is subject to sensor drift and fluid adhering to the sensor tip.*

23. Move the indentation tip to the approximate location of the first grid measurement based on the camera and save the location (Fig 4C and 4D).
24. Move the sensor tip to the region that only contains liquid.
25. Use the "Find Contact" function to automatically detect the fluid surface, then manually lower the sensor further into the fluid about 500 μm.
26. Raise the sensor tip out of contact with the liquid and return the sensor to the saved position.
27. Use the "Find Contact" function to automatically detect the fluid surface, and click "Zero Force", then "Find Contact" to find contact with the biological sample.

    NOTE: *The sensor will automatically raise by 40 μm after this step.*

28. Click "Start Array"; the machine will perform the prescribed array measurement (Fig. 4E).
29. Upon completion of data collection, export indentation data if custom-based data analysis is desired (see Basic Protocol 3); otherwise, use the Data Analysis module that is part of the FemtoTools software program.

BASIC PROTOCOL 3

TISSUE STIFFNESS IDENTIFICATION FROM FORCE-DISPLACEMENT DATA

The objective of this protocol is to outline a procedure to derive sample stiffness, i.e., the apparent elastic modulus, from raw force-displacement data. To that end, we propose a robust algorithm to determine the contact point in force-displacement data from ultrasoft tissue for which the contact point may be difficult to identify (Zhang & Weickenmeier, 2023). Next, we outline two possible approaches to determine sample stiffness based on a well-established parameter optimization approach and a novel machine learning-based approach, respectively. Indentation testing was originally developed to determine the mechanical properties of stiff metals and other solids. Therefore, the most commonly used methods, i.e., the Hertzian contact model, for example, are limited to the linear regime (Hertz, 1881). With the use of indentation testing to characterize soft (biological) materials, the theory was extended to the nonlinear regime and various indenter shapes, i.e., spherical indentation (Lin et al., 2009; Sneddon, 1965). Here, we summarize several common models suitable for spherical indentation that can be used during model parameter optimization (Approach 1) and outline how to apply the machine learning-based approach (Approach 2).

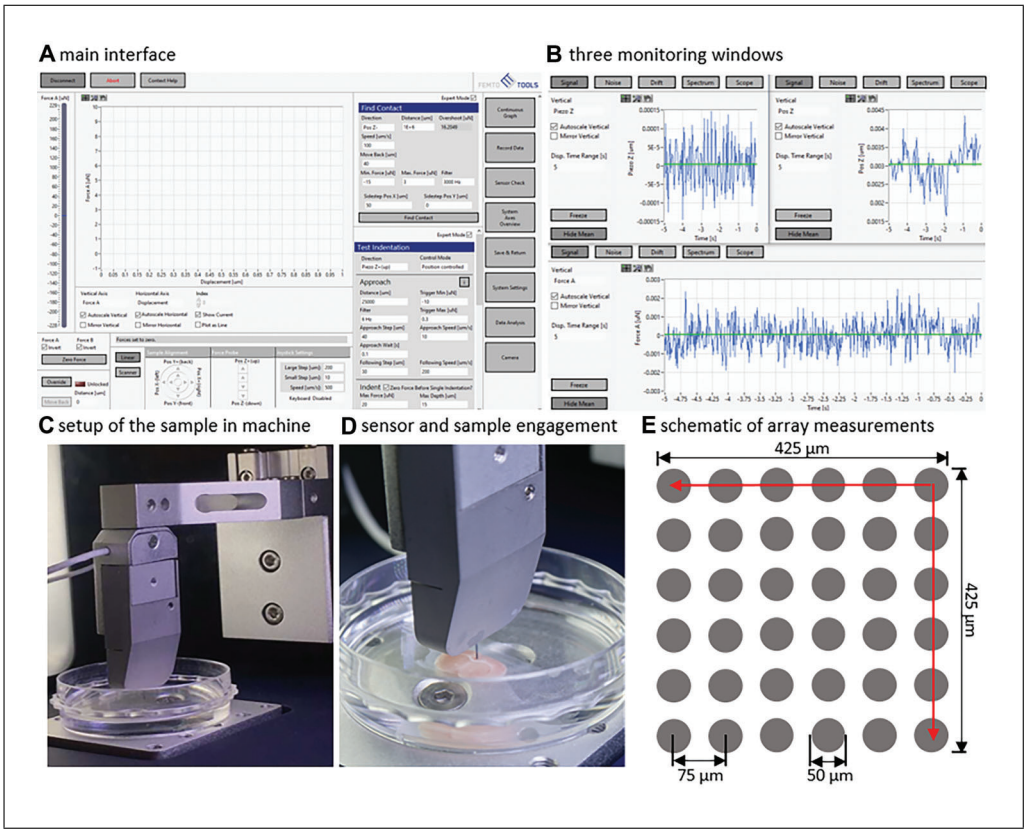

Figure 5 Representative force-displacement curve obtained using Basic Protocol 2. The tip starts out of contact with the sample, approaches the sample (distance d), and switches to displacement-controlled indentation by a prescribed depth when the force sensor exceeds a trigger threshold. We retrospectively determine the actual contact point and only evaluate force-displacement data between the contact point and our desired indentation depth (here set to $\delta = 15$ µm for example).

Weather to use approach 1 or 2 depends on indentation parameters, such as sample dimensions, indentation depth, and bead size. Bead size and indentation depth define the contact radius which subsequently determines the level of strain during indentation (see Approach 1). For brain indentation tests within the linear regime ($\varepsilon < 8\%$), the Hertzian contact model or Sneddon model are commonly used to determine the elastic modulus. For strains exceeding the linear regime (strain $\varepsilon > 8\%$), we select nonlinear models such as the Neo-Hookean, Mooney-Rivlin, Ogden, or Fung model to derive the elastic modulus (see Table 1). Alternatively, Giolando et al.'s machine learning based approach is faster and can be used if the user would like to use either the Neo-Hookean or Gent model and if their experimental protocol fulfills the following conditions: $5 < W/R_s < 40$, $5 < H/R_s < 40$, $0.05 < \delta/R_s < 0.5$, with sample width (W), sample thickness (H), indentation bead radius (R_s), and indentation depth (δ) (Giolando et al., 2023). In this case, we recommend using Approach 2.

Materials

Force-displacement data (see Basic Protocol 2)
Python 3.0 or above
Abaqus

Determining the contact point between indenter tip and sample surface

1. Isolate all data points of the force-displacement data that belong to the loading phase.

   NOTE: *Figure 5 shows a representative force-displacement curve obtained from the FemtoTools FT-MTA03 machine based on our proposed experimental protocol (Basic Protocol 2).*

Table 1 Example of Model Formulations[a]

	Model formulation	Notes
Hertzian (Hertz, 1881)	$F = \frac{4}{3}\frac{E}{1-\nu^2}\frac{a^3}{R_s}$ $a = \sqrt{\delta R_s}$	Linear elastic material assumption
Sneddon (Sneddon, 1965)	$F = \frac{E}{1-\nu^2}\left(\frac{a^2+R_s^2}{2}\ln\frac{R_s+a}{R_s-a} - aR_s\right)$ $\delta = \frac{a}{2}\ln\left(\frac{R_s+a}{R_s-a}\right)$	Linear elastic-perfectly plastic material assumption; provides a better fit for larger deformations compared to the Hertzian model
Mooney-Rivlin (Lin et al., 2009)	$F = B_1\pi\left(\frac{a^5 - 15R_sa^4 + 75{R_s}^2a^3}{5R_sa^2 - 50{R_s}^2a + 125{R_s}^3}\right) + B_2\pi\left(\frac{a^5 - 15R_sa^4 + 75{R_s}^2a^3}{-a^3 + 15R_sa^2 - 75{R_s}^2a + 125{R_s}^3}\right)$ $B_1 + B_2 = \frac{20E}{9\pi(1-\nu^2)}$	Nonlinearly hyperelastic material assumption; it is a reasonable assumption to use the Hertzian definition of contact radius to indentation depth given by $a = \sqrt{\delta R_s}$; a more rigorous representation for this relation is presented by Lin et al. (2009) but requires inverse finite elements
Neo-Hookean (Lin et al., 2009)	$F = B_1\pi\left(\frac{a^5 - 15R_sa^4 + 75{R_s}^2a^3}{5R_sa^2 - 50{R_s}^2a + 125{R_s}^3}\right)$ $B_1 = \frac{20E}{9\pi(1-\nu^2)}$	
Ogden (Lin et al., 2009)	$F = B\pi a^2\left[\left(1-0.2\frac{a}{R_s}\right)^{-\alpha/2-1} - (1-0.2\frac{a}{R_s})^{\alpha-1}\right]$ $B = \frac{40E}{9\pi(1-\nu^2)}$	
Fung (Lin et al., 2009)	$F = B\pi\left(\frac{a^5 - 15R_sa^4 + 75{R_s}^2a^3}{5R_sa^2 - 50{R_s}^2a + 125{R_s}^3}\right) * \exp\left[b\left(\frac{a^3 - 15R_sa^2}{25{R_s}^2a - 125{R_s}^3}\right)\right]$	

[a] Here, F is the indenter force, a is the contact radius, δ is the indentation depth, ν is the Poisson's ratio, R_s is the bead radius, and elastic modulus E.

2. Identify the maximum loading force from the loading phase and then select the n previous measurement points, i.e., in reverse loading direction (towards lower values). We typically use a "sliding window" size of $n = 10$. Calculate the slope of the n measurement points, i.e., the linear fit of the force-displacement data inside the sliding window. Until the determined slope is below a desired threshold, κ, because the loading curve flattens out (see contact point in Fig. 5), iteratively move the sliding window in reverse loading direction until the threshold is crossed. More specifically, re-select n data points from the loading phase, this time starting one data point before the maximum loading force. We typically use a threshold for the slope of $\kappa = 0.008$ μN/μm.

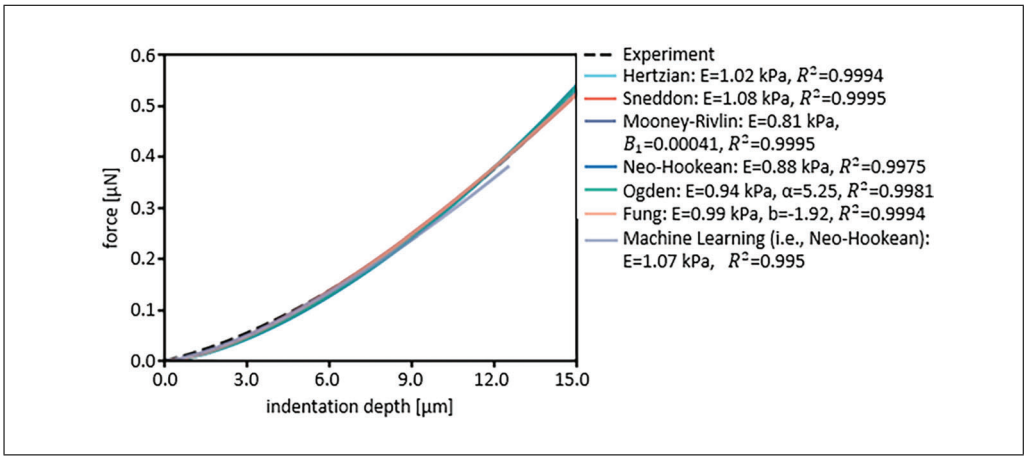

Figure 6 Results from parameter optimization. Here, we fit the equations from Table 1 to the experimental force-displacement data of carpus callosum in mouse brain up to $\delta = 15$ µm.

3. When the threshold is reached, determine the minimum displacement value in the latest data window. We define this point as the contact point between tip and tissue.

   NOTE: *The proposed find contact algorithm works automatically once a suitable window size, n, and slope threshold, κ, have been determined. This depends on the type of force-displacement data the user obtains for their application. We advise, however, to manually check the contact point of each measurement to make manual adjustments to the contact point or possibly discard an individual measurement if the data is inconclusive, i.e., there is either no clear contact point or too much slippage occurred between tip and sample during the loading phase.*

4. Remove all data points prior to the contact point and after the desired indentation depth up to which the user would like to analyze the indentation data; in our application we use a maximum indentation depth of 15 µm.

Approach 1: Parameter optimization to determine tissue stiffness

The parameter optimization approach minimizes the error, e.g., the residual sum of squares, between the experimentally observed force-displacement data and the corresponding model prediction to determine the corresponding parameter(s) that provide(s) an optimal fit between experiment and model. Depending on bead size and indentation depth, the user may choose between a linear (strain $\varepsilon < 8\%$) or nonlinear (strain $\varepsilon > 8\%$) model representation of the indentation experiment. A critical component of the data analysis process is the assumed relationship between indentation depth and contact radius, i.e., the size of the circular area on the sample surface that is in direct contact with the indenter tip. Unless the user chooses the Sneddon model, we recommend working with the formulation derived for linear spherical indentation, $a = \sqrt{\delta R}$, where a is the contact radius, δ is the indentation depth, and R is the bead radius. Strain is given by $\varepsilon = 0.2a/R$ (Lin et al., 2009).

1. Determine the apparent elastic modulus E based on the nonlinear least squares implementation of the SciPy library. To that end, define the residual sum of squares *RSS* given by $RSS = \sum_{i=1}^{n} (y_i - f(\delta_i))^2$, where y_i is the experimentally observed force data and $f(\delta_i)$ is the model predictions based on one of the constitutive relations provided in Table 1, i.e., the Hertzian contact, Sneddon, Mooney-Rivlin, Neo-Hookean, Ogden, and Fung model, respectively. For a comparison of the different models, we fitted them against one of our single indentation measurements in mouse brain, see Figure 6.

NOTE: *The fsolve function uses the default relative error tolerance of 1.49E-8 which the user may wish to change.*

Approach 2: Direct stiffness prediction based on a machine learning approach

This recently proposed machine learning-based approach trained neural networks to inversely identify material parameters of the Neo-Hookean and Gent models from load–displacement curves (*Giolando et al., 2023*). In comparison to conventional methods, this approach is extremely fast and provides excellent fits across a wide range of indentation regimes as well as extreme sample geometries.

1. Download the code from *https://github.com/cmsmlab/AI-dente*
2. Convert your data structure to a nested dictionary and save as a (*).pickle file; for each indentation measurement provide sample thickness, sample width, bead radius, and force-displacement data.
3. Save the reformatted data to the folder "Data/ExperimentalData" as a (*).pickle file.
4. Run the main_AnalyzeData.py file in python, i.e., Pycharm, to determine the material model parameters of each measurement which may be saved as a text file.

NOTE: *You may need to set up the computer environment with optimal version libraries, such as keras 2.13.1, and tensorflow 2.13.0.*

COMMENTARY

Background Information

Brain stiffness values reported in literature continue to vary from study to study. Procurement of samples, sample preparation, and experimental approach all contribute to challenges in reproducing previous work. Mouse brain tissue is significantly more accessible than fresh or fixed human brains, such that it is worthwhile establishing protocols for the preparation of these samples, indentation parameters, and subsequent stiffness evaluation. In the following, we outline critical parameters that should be considered during indentation protocol development in future studies. While some of these considerations are specific to the device we used, their relevance may easily apply to other testing systems we well.

Our grid measurement protocol (Basic Protocol 2) is not without limitations. From experience, we know that force measurements are very sensitive to the interactions between the fluid in which the sample is submerged and detecting the contact point between indentation tip and the surface of ultrasoft tissues such as the brain. Our protocol provides a functioning approach, but other applications may need some adjustments to provide measurement reliability. For example, the type of surfactant, fluid film thickness above the sample, and trigger force are critical parameters that have a significant effect on stiffness measurements and are discussed in the following amongst others. Lastly, our measurements focus on the loading curve alone and we only consider elastic behavior. Additional adjustments to our protocol would be necessary to conduct viscoelastic or other time-dependent tests.

Critical Parameters

Surfactant

Biological tissues should be submerged during testing to prevent dehydration and accelerated cell death. Various buffer solutions have been developed to this effect, including phosphate buffered saline solution, artificial cerebrospinal fluid, HEPES buffered extracellular solution, or deionized water (Antonovaite et al., 2021; Eberle et al., 2020; Habelitz et al., 2002; Urbanski et al., 2019). Indentation devices, however, are very sensitive to these fluids as they affect the sensing mechanisms of most available testing systems. In the case of the FemtoTools FT-MTA03, for example, the sensor gradually enters and exits the fluid bath during each indentation. The corresponding interactions between the fluid's surface tension and indentation probe result in undesired drag and meniscus forces. Therefore, we are required to use a surfactant that minimizes these forces which would otherwise influence the force-displacement curves in each

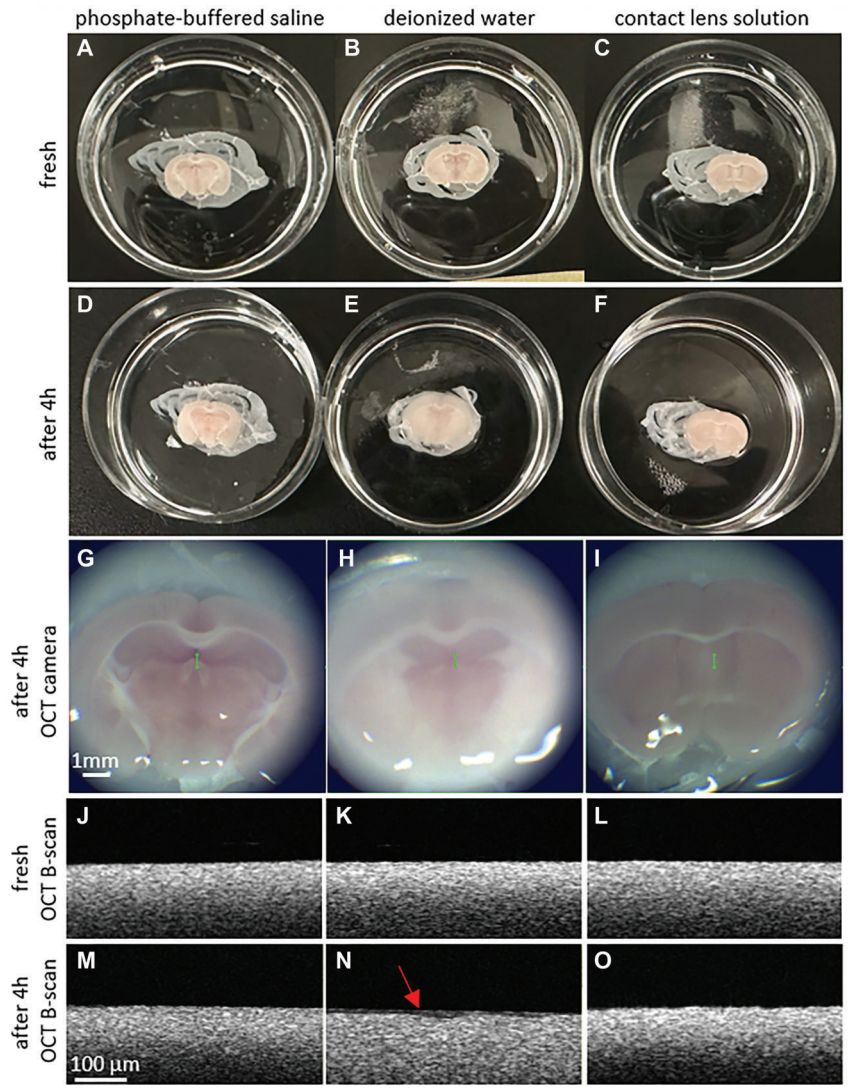

Figure 7 Effect of surfactant exposure time on sample surface. We harvested three coronal mouse brain slices and used OCT imaging to assess swelling between harvest and 4 hr of submersion in fluid. Figures (**A-C**) show digital photos of fresh slices immediately after obtaining them from a mouse brain and (**D-F**) shows the same slices after 4 hr in either phosphate-buffered saline, deionized water, and contact lens solutions respectively. The OCT camera already indicates swelling based on the increase in blurriness after 4 hr in the respective solutions (**G-I**). OCT B-scan images for fresh brain slices (**J-L**), and the same slices after 4 hr (**M-O**).

measurement depending on the amount of fluid in the petri dish.

We propose using contact lens solution, as it is biocompatible and effectively reduced drag forces during our tests. To better understand the effect of surfactant on tissue surface changes, we harvested a 1000-µm thick coronal slice from three different mice. As shown in Figure 7, each slice was glued to the bottom of a petri dish and then submerged with either (a) phosphate-buffered saline (PBS), (b) deionized water, or (c) contact lens solution. We then used optical coherence tomography (OCT) to visualize the top layers of the freshly obtained brain slices immediately after harvesting and a second time 4 hr later, see Figure 7D-F, respectively. From the OCT camera view alone, it is evident that the slice submerged in deionized water exhibited significant swelling (Fig. 7H). The slices placed in PBS and contact lens solution showed much less swelling during the same time window (Fig. 7G and 7I), respectively. OCT measurements show the swelling behavior when comparing fresh (Fig. 7J-L) and late stage (Fig. 7M-O). The red arrow in Figure 7N highlights

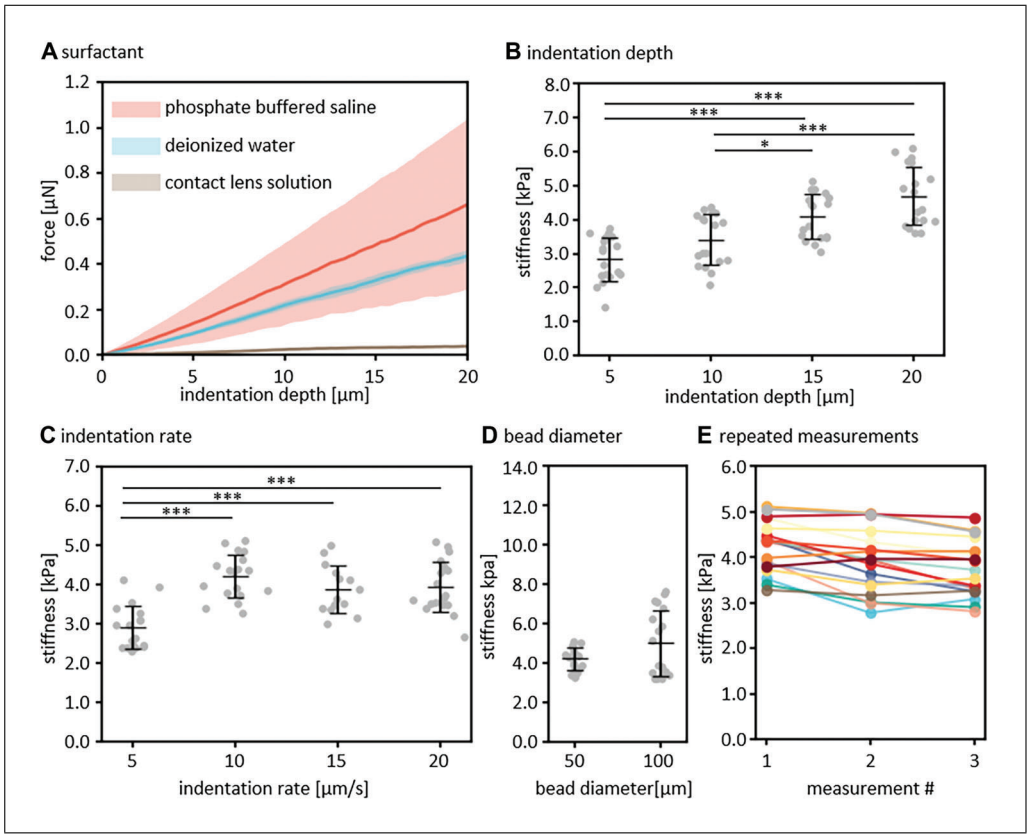

Figure 8 Parameter sensitivity analysis with respect to (**A**) fluid used to submerge the sample, i.e., surfactant, (**B**) indentation depth, (**C**) indentation rate, (**D**) bead diameter, and (**E**) stiffness (i.e., elastic modulus) changes with repeated measurements in the same location.

the surface swelling of the slice in deionized water after 4 hr reflected in the more diffuse superficial layer (top microns). Swelling is also evident in the images after 4 hr where the OCT image cannot penetrate the full swollen sample (Fig. 7N).

To demonstrate the effect of reducing drag forces using contact lens solution, we report tip forces when submerging the probe in deionized water, phosphate buffered solution, and Opti-Free Contact Lens Solution (Fig. 8A). In this test, we first determined the contact point with the fluid, inserted the probe by another 200 µm such that the bead is fully submerged, and then performed a 20 µm indentation. Figure 8A shows that the sensor force gradually increases as the probe moves into water and PBS, while the contact lens solution effectively prevents drag forces. Over the entire indentation depth, we observed a mean slope of 0.0338 ± 0.0186 µN/µm in PBS, 0.0227 ± 0.0014 µN/µm in water, and 0.0020 ± 0.0003 µN/µm in contact lens solution. *It is important to note*, however, that contact lens solution may inadvertently influence cell integrity; especially so, if an extended testing time is required for large grid measurements.

Indentation depth

Selecting indentation depth depends on various factors including indenter (bead) size, sample thickness, and sample stiffness. Typically, the softer the material, the more difficult it becomes to reliably detect the contact point between sample and tissue. This can be compensated for by prescribing larger indentation depths. However, one easily exceeds the linear regime as strains quickly go beyond 8% (Antonovaite et al., 2021). We assessed the effect of indentation depth on stiffness by performing a total of 72 measurements in the cortex with indentation depths of 5 µm, 10 µm, 15 µm, and 20 µm, respectively. We evaluated force-displacement data based on the Sneddon model. Figure 8B shows that stiffness gradually increases with increasing indentation depth although statistical significance was not established between all the groups. Specifically, mean stiffness increases from 2.8 ± 0.6 kPa for 5 µm indentation depth, to 3.4 ± 0.7 kPa at 10 µm, 4.1 ± 0.7 kPa at 15 µm, and 4.7 ± 0.9 kPa at 20 µm.

Indentation rate

Different indentation rates allow to quantify the time-dependent tissue response and

simulate various physiological conditions. Dynamic testing with a high indentation rate may mimic more rapid physiological processes, while quasi-static testing with a low rate can represent slower, more gradual changes. We evaluated the effect of indentation rate on the quasi-static stiffness measurement by prescribing indentation rates of 5 μm/s, 10 μm/s, 15 μm/s, and 20 μm/s. Figure 8C shows a mean stiffness of 2.9 ± 0.5 kPa at 5 μm/s, which then stabilizes around 4.0 ± 0.6 kPa. A similar indentation rate-dependent behavior was observed before (Budday et al., 2015; Van Dommelen et al., 2010).

Bead size

Bead size determines the length scale at which the material is probed. Here, we evaluated two different bead sizes, i.e., 50 μm and 100 μm, and measured tissue stiffness in 18 different cortical locations. Figure 8D shows that stiffness increased from 4.2 ± 0.5 kPa to 5.5 ± 1.7 kPa with increasing bead size. It appears that measurements with the larger bead result in pronounced stiffness variations (reflected in larger standard deviation), which may be associated with recruiting more heterogeneous materials in comparison to the smaller bead. Therefore, no statistical difference ($p = 0.066$) with respect to bead size was observed in this case.

Repeated measurements in the same location

Repeated measurements in the same location may precondition the tissue and affect stiffness values. To evaluate stiffness changes upon repeated indentation, we harvested two mouse brains and performed three consecutive indentations in 18 individual locations in the cortex. We perform a Mann-Kendall test at each location to evaluate a possible trend in stiffness values across the three repeated indentations. We did not observe any statistically significant difference at any of the 18 locations ($p > 0.1$), which suggests that tissue stiffness appears to be unaffected by repeated measurements in the same location (Fig. 8E). We suspect that the combination of a rather large bead size and rather slow indentation depths lead to quickly recoverable tissue deformations between individual measurements.

Troubleshooting

Surfactant evaporation during testing

We propose using contact lens solution for its reliable reduction in drag forces on the sensor tip. However, during prolonged measurement series, fluid on the sensor tip may evaporate and leave residual solids that create a new source for drag forces. To reduce the impact of this effect, we recommend inputting all indentation parameters in the FemtoTools interface before preparing the sample such that the device is ready for immediate testing. Additionally, once the sample is ready, we keep the sensor tip wet by lowering it by 1500 μm into contact lens solution before any measurement series (see Basic Protocol 2, steps 6-10).

Move back distance, approach step size, and follow-up step size

Despite our robust sample preparation procedure, our samples have an inherent surface roughness that we must account for during indentation measurements. Especially, when performing grid measurements, each individual measurement must start with sufficient clearance between the indenter tip and sample surface such to avoid undesired contact when moving the tip laterally to the next measurement location. The amount of clearance is defined by the move-back distance parameter. This limitation also means, however, that during each indentation, the machine must automatically switch from the "approach mode" (during which it tries to find the sample surface) to displacement-controlled "indentation mode" (to probe the sample up to the desired indentation depth). Specifically, during the approach phase, the machine lowers the probe by the prescribed approach step size; if the prescribed trigger force threshold is not reached, the machine will rise the probe by the follow-up step size (which is smaller than the approach step size). This approach step is repeated by the machine until the trigger force is exceeded (which indicates that the probe is in contact with the sample). The machine then switches to the indentation mode. The following challenges should further be considered:

• Given the potential drag forces on the probe while it lowers into fluid, prescribing a low trigger force that is too low will cause a premature switch from approach mode to indentation mode. Too high of a trigger force will cause the probe to (potentially) extensively penetrate the sample before switching to the desired indentation mode, which causes indentation beyond the desired depth. Additionally, there is the risk of deforming or breaking the tip.

• The FT-MTA03 is limited in terms of maximum tip movement (linear stage plus piezo) during a single approach step. It is disadvantageous when the trigger force is reached

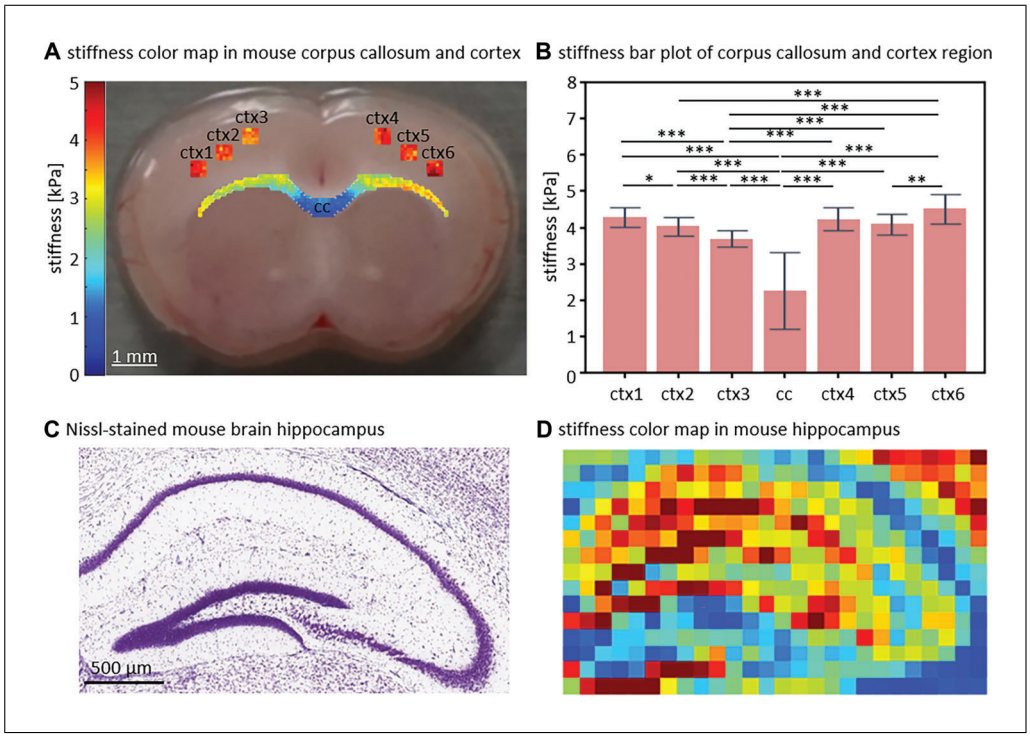

Figure 9 Application of indentation on fresh soft tissues, (**A**) averaged heat map of the heterogeneous stiffness (i.e., elastic modulus) distribution in corpus callosum (cc) and cortex (ctx) based on three samples, (**B**) bar plot of the stiffness in the corpus callosum ($n = 945$ measurements) and six cortical subregions ($n_1 = 75$, $n_2 = 75$, $n_3 = 75$, $n_4 = 75$, $n_5 = 75$, and $n_6 = 75$ measurements per subregion, respectively), (**C**) Nissl-stained mouse brain hippocampus from the Allen Brain Atlas (available at *http://www.brain-map.org*), (**D**) corresponding stiffness map of the mouse hippocampus (one sample, $n = 390$ measurements) obtained by indentation (same color bar as subfigure a). *** indicates $p < 0.005$, ** indicates $p < 0.01$, and * indicates $p < 0.05$.

at the end of the maximum possible tip movement during an approach step. Therefore, approach step size, follow-up step size, and trigger force need to be carefully selected to ensure reliable indentation in very soft tissues.

Understanding Results

Our protocols enable microscale indentation testing of mouse brain tissues and outline suitable strategies to determine tissue stiffness. We have used our protocols to measure spatial stiffness variations as well as the impact of microstructural changes on region-specific tissue stiffness (Zhang & Weickenmeier, 2023). In the mouse brain, the cortical layer, i.e., gray matter, is significantly stiffer than the subcortical layer, i.e., white matter. At the same time, we commonly observe that there are substantially lower spatial stiffness variations in gray matter in comparison to white matter. Specifically, Figure 9A and 9B show that the corpus callosum in mice is up to 4 times softer than gray matter, and around 2.5× softer than the lateral region of white matter. Results were obtained using Approach 1 from Basic Protocol 3 using the Sneddon model, see Table 1. We can also show that our approach provides high spatial resolution for the example of the mouse hippocampus as shown in Figure 9C and 9D. The comparison between the histochemical staining and the stiffness heat map reveals a good spatial overlap with anatomical subregions.

Time Considerations

3D printing of the cutting mold may take several hours depending on the printer and settings. Using our machine, it took 2 hr to print the mold with an in-plane resolution of 100 µm and a layer thickness of 0.2 mm.

Gluing the bead to the tip of the indenter may take up to 15 min. Manually identifying a bead and positioning the indenter tip perfectly above the center of the bead requires a few minutes. Once the position of the bead is saved, dipping the tip in glue, and returning to the bead takes less than a minute. Right afterwards, the adhesive needs to be cured with UV light for 1 minute.

Sample preparation may take up to 15 min since it requires (1) sacrificing the mouse, (2)

removing the brain from the skull, (3) mounting for cutting with the vibratome, and (4) transferring to the petri dish.

The total mechanical testing time depends on the grid size. With our current settings, a single measurement takes 10 s to complete, and about 6 min for a 6 × 6 array. In a recent study (Zhang & Weickenmeier, 2023), we tested 72 locations in the corpus callosum, 36 locations in the cingulum, and 36 locations in the cortex and required 24 min of pure testing time. Additional time is required to transfer the sample, place it in the machine, adjust lighting and the microscope, initialize the probe, identify the desired array location, and add surfactant to the sample. Overall, we expect the three arrays with 144 measurements to require 60 min for a single sample.

Acknowledgments

This study was supported by the National Science Foundation under grant number 1953323 to Johannes Weickenmeier.

Author Contributions

Xuesong Zhang: Conceptualization; data curation; methodology; writing—original draft. **Eva van den Hurk:** Data curation; methodology. **Johannes Weickenmeier:** Conceptualization; methodology; writing—original draft.

Conflict of Interest

The authors declare no conflict of interest.

Data Availability Statement

Data presented here will be made available upon request.

Literature Cited

Antonovaite, N., Beekmans, S., Hol, E., Wadman, W., & Iannuzzi, D. (2018). Regional variations in stiffness in live mouse brain tissue determined by depth-controlled indentation mapping. *Scientific Reports*, *8*(1), 12517. https://doi.org/10.1038/s41598-018-31035-y

Antonovaite, N., Hulshof, L., Hol, E., Wadman, W., & Iannuzzi, D. (2021). Viscoelastic mapping of mouse brain tissue: Relation to structure and age. *Journal of the Mechanical Behavior of Biomedical Materials*, *113*, 104159. https://doi.org/10.1016/j.jmbbm.2020.104159

Blinkouskaya, Y., Caçoilo, A., Gollamudi, T., Jalalian, S., & Weickenmeier, J. (2021). Brain aging mechanisms with mechanical manifestations. *Mechanisms of Ageing and Development*, *200*, 111575. https://doi.org/10.1016/j.mad.2021.111575

Budday, S., Nay, R., de Rooij, R., Steinmann, P., Wyrobek, T., Ovaert, T., & Kuhl, E. (2015). Mechanical properties of gray and white matter brain tissue by indentation. *Journal of the Mechanical Behavior of Biomedical Materials*, *46*, 318–330. https://doi.org/10.1016/j.jmbbm.2015.02.024

Budday, S., Ovaert, T., Holzapfel, G., Steinmann, P., & Kuhl, E. (2020). Fifty shades of brain: A review on the mechanical testing and modeling of brain tissue. *Archives of Computational Methods in Engineering*, *27*(4), 1187–1230. https://doi.org/10.1007/s11831-019-09352-w

Budday, S., Sommer, G., Birkl, C., Langkammer, C., Haybaeck, J., Kohnert, J., & Kuhl, E. (2017). Mechanical characterization of human brain tissue. *Acta Biomaterialia*, *48*, 319–340. https://doi.org/10.1016/j.actbio.2016.10.036

Christ, A., Franze, K., Gautier, H., Moshayedi, P., Fawcett, J., Franklin, R., Karadottir, R., & Guck, J. (2010). Mechanical difference between white and gray matter in the rat cerebellum measured by scanning force microscopy. *Journal of Biomechanics*, *43*(15), 2986–2992. https://doi.org/10.1016/j.jbiomech.2010.07.002

Eberle, D., Fodelianaki, G., Kurth, T., Jagielska, A., Möllmert, S., Ulbricht, E., Wagner, K., Taubenberger, A., Träber, N., Escolano, J., Vliet, K., & Guck, J. (2020). Acquired demyelination but not genetic developmental defects in myelination leads to brain tissue stiffness changes. *Brain Multiphysics*, *1*, 100019. https://doi.org/10.1016/j.brain.2020.100019

Faber, J., Hinrichsen, J., Greiner, A., Reiter, N., & Budday, S. (2022). Tissue-scale biomechanical testing of brain tissue for the calibration of nonlinear material models. *Current Protocols*, *2*(4), e381. https://doi.org/10.1002/cpz1.381

Franze, K., Janmey, P., & Guck, J. (2013). Mechanics in neuronal development and repair. *Annual Review of Biomedical Engineering*, *15*, 227–251. https://doi.org/10.1146/annurev-bioeng-071811-150045

Gefen, A., & Margulies, S. (2004). Are in vivo and in situ brain tissues mechanically similar? *Journal of Biomechanics*, *37*(9), 1339–1352. https://doi.org/10.1016/j.jbiomech.2003.12.032

Giolando, P., Kakaletsis, S., Zhang, X., Weickenmeier, J., Castillo, E., Dortdivanlioglu, B., & Rausch, M. (2023). AI-dente: An open machine learning based tool to interpret nano-indentation data of soft tissues and materials. *Soft Matter*, https://doi.org/10.1039/D3SM00402C

Goriely, A., Geers, M., Holzapfel, G., Jayamohan, J., Jérusalem, A., Sivaloganathan, S., Squier, W., van Dommelen, J., Waters, S., & Kuhl, E. (2015). Mechanics of the brain: Perspectives, challenges, and opportunities. *Biomechanics and Modeling in Mechanobiology*, *14*, 931–965. https://doi.org/10.1007/s10237-015-0662-4

Guimarães, C., Gasperini, L., Marques, A., & Reis, R. (2020). The stiffness of living tissues and its implications for tissue engineering. *Nature Reviews Materials*, *5*(5), 351–370. https://doi.org/10.1038/s41578-019-0169-1

Habelitz, S., Marshall, G. W. Jr., Balooch, M., & Marshall, S. J. (2002). Nanoindentation and

storage of teeth. *Journal of Biomechanics*, *35*(7), 995–998. https://doi.org/10.1016/S0021-9290(02)00039-8

Hall, C., Moeendarbary, E., & Sheridan, G. (2021). Mechanobiology of the brain in ageing and Alzheimer's disease. *European Journal of Neuroscience*, *53*(12), 3851–3878. https://doi.org/10.1111/ejn.14766

Hertz, H. (1881). The contact of elastic solids. *Journal fur die Reine und Angewandte Mathematik*, *92*, 156–171.

Hiscox, L., Johnson, C., McGarry, M., Marshall, H., Ritchie, C., Beek, E., Roberts, N., & Starr, J. (2020). Mechanical property alterations across the cerebral cortex due to Alzheimer's disease. *Brain Communications*, *2*(1), fcz049. https://doi.org/10.1093/braincomms/fcz049

Lin, D., Shreiber, D., Dimitriadis, E., & Horkay, F. (2009). Spherical indentation of soft matter beyond the Hertzian regime: Numerical and experimental validation of hyperelastic models. *Biomechanics and Modeling in Mechanobiology*, *8*(5), 345–358. https://doi.org/10.1007/s10237-008-0139-9

Luo, Q., Kuang, D., Zhang, B., & Song, G. (2016). Cell stiffness determined by atomic force microscopy and its correlation with cell motility. *Biochimica et Biophysica Acta (BBA)-General Subjects*, *1860*(9), 1953–1960. https://doi.org/10.1016/j.bbagen.2016.06.010

MacManus, D., & Ghajari, M. (2022). Material properties of human brain tissue suitable for modelling traumatic brain injury. *Brain Multiphysics*, 100059. https://doi.org/10.1016/j.brain.2022.100059

Meaney, D., Morrison, B., & Dale Bass, C. (2014). The mechanics of traumatic brain injury: A review of what we know and what we need to know for reducing its societal burden. *Journal of Biomechanical Engineering*, *136*(2), 021008. https://doi.org/10.1115/1.4026364

Moghaddam, A., Arshee, M., Lin, Z., Sivaguru, M., Phillips, H., McFarlin, B., Toussaint, K., & Wagoner, A. (2023). Orientation-dependent indentation reveals the crosslink-mediated deformation mechanisms of collagen fibrils. *Acta Biomaterialia*, *158*, 347–357. https://doi.org/10.1016/j.actbio.2023.01.005

Murphy, M., Curran, G., Glaser, K., Rossman, P., Huston, J. III., Poduslo, J., Clifford, R., Felmlee, J., & Ehman, R. (2012). Magnetic resonance elastography of the brain in a mouse model of Alzheimer's disease: Initial results. *Magnetic Resonance Imaging*, *30*(4), 5 35–539. https://doi.org/10.1016/j.mri.2011.12.019

Sneddon, I. (1965). The relation between load and penetration in the axisymmetric Boussinesq problem for a punch of arbitrary profile. *International Journal of Engineering Science*, *3*(1), 47–57. https://doi.org/10.1016/0020-7225(65)90019-4

Urbanski, M., Brendel, M., & Melendez-Vasquez, C. (2019). Acute and chronic demyelinated CNS lesions exhibit opposite elastic properties. *Scientific Reports*, *9*(1), 999. https://doi.org/10.1038/s41598-018-37745-7

van Dommelen, J., van der Sande, T., Hrapko, M., & Peters, G. (2010). Mechanical properties of brain tissue by indentation: Interregional variation. *Journal of the Mechanical Behavior of Biomedical Materials*, *3*(2), 158–166. https://doi.org/10.1016/j.jmbbm.2009.09.001

Weickenmeier, J., de Rooij, R., Budday, S., Steinmann, P., Ovaert, T., & Kuhl, E. (2016). Brain stiffness increases with myelin content. *Acta Biomaterialia*, *42*, 265–272. https://doi.org/10.1016/j.actbio.2016.07.040

Zhang, X., & Weickenmeier, J. (2023). Brain stiffness follows cuprizone-induced variations in local myelin content. *Acta Biomaterialia*, https://doi.org/10.1016/j.actbio.2023.08.033